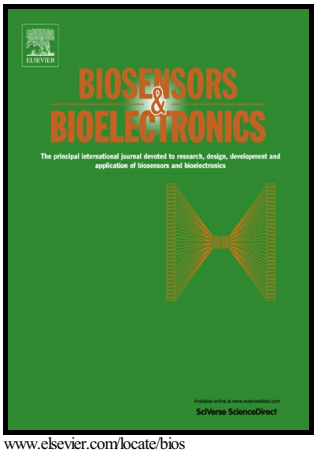

www.elsevier.com/locate/bios

Hierarchical porous microspheres of the Co_3O_4@graphene with enhanced electrocatalytic performance for electrochemical biosensors

MinHo Yang, Jae-Min Jeong, Kyoung G. Lee, Do Hyun Kim, Seok Jae Lee, Bong Gill Choi

PII: S0956-5663(16)30087-2
DOI: http://dx.doi.org/10.1016/j.bios.2016.01.075
Reference: BIOS8415

To appear in: *Biosensors and Bioelectronic*

Received date: 11 November 2015
Revised date: 1 January 2016
Accepted date: 28 January 2016

Cite this article as: MinHo Yang, Jae-Min Jeong, Kyoung G. Lee, Do Hyu Kim, Seok Jae Lee and Bong Gill Choi, Hierarchical porous microspheres of th Co_3O_4@graphene with enhanced electrocatalytic performance fo electrochemical biosensors, *Biosensors and Bioelectronic* http://dx.doi.org/10.1016/j.bios.2016.01.075

Hierarchical porous microspheres of the Co_3O_4@graphene with enhanced electrocatalytic performance for electrochemical biosensors

MinHo Yang,[†] Jae-Min Jeong,[‡] Kyoung G. Lee,[†] Do Hyun Kim,[‡] Seok Jae Lee,[*,†] and Bong Gill Choi[*,§]

[†] Department of Nano Bio Research, National NanoFab Center (NNFC), Daejeon 305-806, Republic of Korea

[‡] Department of Chemical & Biomolecular Engineering, Korea Advanced Institute of Science and Technology (KAIST), Daejeon 305-701, Republic of Korea

[§] Department of Chemical Engineering, Kangwon National University, Samcheok 245-711, Republic of Korea

*Co-corresponding Authors

*E-mail: sjlee@nnfc.re.kr

*E-mail: bgchoi@kangwon.ac.kr

Fax: +82-33-570-6535

Tel: +82-33-570-6545

Abstract

The integration of organic and inorganic building blocks into hierarchical porous architectures makes potentially desirable electrocatalytic materials in many electrochemical applications due to their combination of attractive qualities of dissimilar components and well-constructed charge transfer pathways. Herein, we demonstrate the preparation of the hierarchical porous Co_3O_4@graphene (Co_3O_4@G) microspheres by one-step hydrothermal method to achieve high electrocatalytic performance for enzyme-free biosensor applications. The obtained Co_3O_4@G microspheres are consisted of the interconnected networks of Co_3O_4 and graphene sheets, and thus provide large accessible active sites through porous structure, while graphene sheets offer continuous electron pathways for efficient electrocatalytic reaction of Co_3O_4. These structural merits with synergy effect of Co_3O_4 and graphene lead to a high performance of enzyme-free detection for glucose: high sensitivity, good selectivity, and remarkable stability.

KEYWORDS: Nanocomposite, Graphene, Metal oxide, Electrochemical biosensor

1. Introduction

The hierarchical porous architectures constructed from nanoscale primary blocks with specific dimensions have received a great deal of attention because of their exceptional properties and numerous promising applications in a wide range of fields (Cong et al., 2014; Hu and Chen 2014; Hamon et al., 2014). In particular, hierarchical porous nanocomposites assembled with metal oxides and conductive agents (e.g., conducting polymers, carbon nanotubes, and graphene) (Sumathi et al., 2014; Wang et al., 2014; Yue et al., 2014; Xiao et al., 2012) have been considered potential electrode materials for high-performance electrochemical biosensors due to their large accessible surface areas and improved kinetic transport properties. The continuous conductive networks also provide efficient electron pathways between active sites and electrodes, which allow rapid electron transfer and concomitantly enhance performance indicators, such as sensitivity, limit of detection, and response time.

To date, most electrochemical biosensors have adopted enzyme-based electrodes that employ glucose oxidase (Chen et al., 2013), horseradish peroxidase (Zen et al., 2010) or hemoglobin (Baghayeri et al., 2015) as catalysts for target oxidation or reduction. Although there have already been tremendous benefits from the use of enzyme-based electrodes, the insufficient stability and unsatisfactory reproducibility may restrict the shelf life of other sensor systems (Wilson and Turner., 1992). Non-enzymatic electrochemical biosensors have been considered an attractive alternative for the use of enzymes due to their reduced cost, increased stability, robustness, and recyclability (Si et al., 2013). Over the past few decades, noble metals (e.g., Pt, Au, and Pd) (Park et al., 2003; Cheng et al., 2010; Chen et al., 2010) and alloys (e.g., Pt–Pb, Pt–Cu, Pt–Au, and etc) (Wang et al., 2008; Cao et al., 2013; Xiao et al., 2009; Cao et al., 2011) have been explored as a non-enzymatic electrode for direct electrocatalytic oxidation of glucose.

However, these electrodes often have drawbacks such as low sensitivity and poor stability caused by surface poisoning from the adsorbed intermediates and chloride (Toghill and Compton., 2010). Recently, nanostructured metal oxides (e.g., Co_3O_4, NiO, CuO, and Mn_3O_4) (Lang et al., 2013; Ding et al., 2010; Mu et al., 2011; Reitz et al., 2008; Si et al., 2013) have attracted considerable attention due to their excellent electrocatalytic activity toward glucose and H_2O_2 oxidation. Although the nanostructured metal oxides (NMOs) could provide superior amperometric sensing performance over a wide range of glucose concentrations, their low intrinsic electrical conductivity (for example, Co_3O_4 in $\sim 10^{-5}$ S m^{-1} at room temperature) (Lang et al., 2013) impedes their widespread use in electrochemical biosensor devices that require high sensitivity, reliability, fast response, and excellent selectivity. One of the most attractive approaches is to incorporate NMOs into graphene sheets that are highly conductive and have a large surface area. For instance, Zheng et al. synthesized 2D nanocomposites composed of Co_3O_4 nanoparticles and graphene sheets (Zheng et al., 2014). However, these 2D nanocomposites limited ion transfer during electrochemical reactions. To address these issues, 3D porous conductive supports have been employed for deposition of cobalt oxides including graphene foams synthesized by chemical vapor deposition and graphene hydrogels prepared by hydrothermal method (Dong et. al., 2012; Hoa et al., 2016; Wang et al., 2012) and these studies have resulted in significant improvement of non-enzymatic glucose sensing performance. Despite these efforts, the preparation of porous cobalt oxide/graphene composites still require complicated equipment and/or multi-step procedure, which are not applicable for cost-effective and scalable electrochemical biosensors.

Herein, we report a simple synthesis for preparation of hierarchical porous Co_3O_4@graphene (Co_3O_4@G) microspheres by in situ self-assembly of Co_3O_4 nanosheets and

graphene sheets for high performance of enzyme-free electrochemical biosensors. The resulting Co_3O_4@G microspheres showed well-defined hierarchical porous structures with enhanced electrical conductivity and large surface area. Owing to the unique features of the as-prepared Co_3O_4@G microsphere, excellent electrochemical performance was expected because of the rapid and sufficient mass transfer and electron transfer within the materials. Flow-injection system was constructed to evaluate electrocatalytic performance of Co_3O_4@G microspheres, showing high sensitivity, low limit of detection, fast response time, and high selectivity toward glucose detection in an alkaline medium.

2. Experimental section

2.1. Preparation of Co_3O_4@G microsphere

As starting materials, GOs were first prepared through a modified Hummers method as described in our previous report (Choi et al., 2010). The Co_3O_4@G microsphere were fabricated using the one-step hydrothermal method. $Co(NO_3)_2 \cdot 6H_2O$ (1 mM) and 40 mg of GOs were dispersed in 15 mL of deionized (DI) water. After sonication for 10 min, the ethylene diamine was added dropwise into the above solution with continuous sonication for 3 min. The well dispersed mixture was sealed in 18 mL Teflon-line autoclave and maintained at 90 °C. After a reaction time of 12 hr, the resulting samples were filtered and washed several times with water. Finally, the CoO_x@G microspheres were freeze-dried for a 1 day in order to remove water without destroying their structure. These samples were then annealed at 350 °C for 1 hr to complete Co_3O_4@G microsphres.

2.2. Preparation of Co_3O_4@G microsphere modified electrode

Before surface modification, glassy carbon electrode (GCE, dia 3 mm) was polished with 0.05 μm alumina sequentially, and then rinsed with DI water. Finally, the electrode was sonicated in

ethanol and deionized water, dried at room temperature, and ready for modification. To prepare 5 mg mL^{-1} of Co_3O_4@G suspension, Co_3O_4@G (5 mg) was first suspended in 1 mL ethanol and sonicated for 1 hr. Next, a 5 μL Co_3O_4@G suspension was dropped onto the surface of GCE. After drying in air, an aliquot of 5 μL Nafion solution (1 wt% in propanol) was casted on the layer of Co_3O_4@G in order to entrap Co_3O_4@G. The as-prepared electrode was immersed in DI water for 1 hr to wet the Nafion layer thoroughly before use. The Co_3O_4 coated GCE was also prepared as a control electrode.

2.3. Characterization

Transmission electron microscopy (TEM) measurements were carried out using a JEM-2100F high- resolution TEM (HR-TEM) at an acceleration voltage of 200 kV. The SEM images were obtained using a field emission scanning electron microscopy (SEM, S-4800) equipped with a Schottky emitter in high stability. X-ray diffraction (XRD) pattern was obtained on a Rigaku D/MAX-2500 (40 kV, 300 mA, Cu Kα radiation). X-ray photoelectron spectroscopy (XPS) measurement was conducted using a Thermo MultiLab 2000 system. The Raman spectra were obtained using an ARAMIS Spectra spectrometer (Horiba Jobin Yvon, France). Cyclic voltammetry (CV) and electrochemical impedance spectroscopy (EIS) were performed using a VersaSTAT 4 (Princeton Applied Research) electrochemical workstation. For testing purposes, a conventional three-electrode electrochemical cell was employed with a glassy carbon working electrode, an Ag/AgCl (3 M KCl) reference electrode, and a platinum wire counter electrode. All potentials were recorded with respect to the reference electrode. EIS was carried out in the range of 0.01 Hz to 100 kHz at constant amplitude of 10 mV. In order to evaluate the sensing performance, a flow injection microfluidic system was set up using a syringe pump (KD scientific, KDS 100) and a sample injector (Rhoedyne, model 7725i) with a 5 μL sample loop.

The microfluidic device was assembled with working, counter, and reference electrodes in a plastic case. A Teflon gasket with a flow channel was sandwiched between the working electrode and the plastic case in order to provide sufficient contact between the sample and the Co_3O_4@G. The amperometric technique was carried out in this flow injection system to detect glucose molecules injected at a flow rate of 500 μL min^{-1}. All of the electrochemical measurements were performed at room temperature. The electrolyte was 0.1 M NaOH solution for all electrochemical measurements in order to maintain optimal stability of Co_3O_4 for glucose oxidation.

3. Results and discussion

3.1. Synthesis and characterization of Co_3O_4@G microspheres

The hierarchical porous Co_3O_4@G microspheres was prepared by one-step hydrothermal method, in which homogeneous graphene oxide (GO) aqueous solution was mixed with Co precursors and ethylene diamine as a reducing agent in a Teflon-lined autoclave and the mixture was treated at 90 °C for 12 hr. The morphology and microstructure of Co_3O_4@G microsphere were examined by SEM and TEM images (Fig. 1). The Co_3O_4@G was consisted of relatively uniform flower-like microspheres with an average diameter of 8.2 ± 1.6 μm (Fig. 1a and Fig. S1). Furthermore, the enlarged SEM image shows that flower-like microspheres were assembled by a large number of nanosheets (Fig. 1b). A strong mutual interaction between the Co_3O_4 and graphene sheets triggered hierarchical co-assembly of microspherical structure in order to minimize surface energy. The hydrothermal process using Co precursor alone led to hexagonal nanosheets rather than hierarchical microsphere structure (Fig. S2). Energy dispersive spectroscopy (EDS) analysis confirmed coexistence of Co_3O_4 and graphene sheets from strong carbon and cobalt signals (Fig. 1c). A high-resolution TEM image revealed that the graphene

nanosheets were aggregated and interconnected with Co_3O_4 nanosheets into microspheres (Fig. 1d). The EDS mapping of microspheres (Fig. 1e) indicated that uniform distribution of Co, O, and C, confirming the coexistence and homogeneous distribution of cobalt oxide on graphene sheets. Obviously, the carbon signal for graphene and the cobalt signal for Co_3O_4 overlapped uniformly across the entire microsphere. The powder XRD pattern of Co_3O_4@G (Fig. 1f) shows (111), (220), (311), (511) and (440) diffraction peaks, which can indexed as the face-centered cubic structure of Co_3O_4 (JCPDS, Card No. 42-1467). Compared to that of pure Co_3O_4 (Fig. S3), the additional broad peak at 2θ = 22–24° must be attributed to the disordered stacking of the graphene sheet (Choi et al., 2010). Raman spectra of Co_3O_4@G displays two prominent peaks at about 1353 and 1599 cm^{-1} (Fig. S4), which correspond to the D and G bands of graphene sheet, respectively (Hoa et al., 2016). Moreover, five peaks at 195, 484, 522, 620, and 690 cm^{-1} can be assigned to Co_3O_4 (Yang et al., 2010). The XRD and Raman anlaysis further confirm the sucessful hybridization of graphene and Co_3O_4.

The chemical composition of the Co_3O_4@G was further investigated by XPS measurements. The survey spectrum clearly show the presence of C, O, and Co elements in the Co_3O_4@G compared with GO, suggesting the thin coating of Co_3O_4 onto graphene sheets (Fig. 2a). Deconvolution of the C 1s peak of the Co_3O_4@G in Figure 2b displays three types of carbon bonds: C−C (284.7 eV), C−O (286.1 eV), and C=O (288.1 eV) (Yang et al., 2009). Compared to GOs (Fig. S5), the intensity of oxygen functional groups of Co_3O_4@G, such as epoxy/hydroxyl and carbonyl groups decreased dramatically due to the efficient deoxygenation and reduction during the hydrothermal process. The regional Co 2p spectrum in Fig. 2c shows a high energy band at 795.4 eV (Co $2p_{1/2}$) and a low energy band at 780.2 eV (Co $2p_{3/2}$), which was in accordance with that reported for Co_3O_4 (Li et al., 2014). The presence of two shakeup satellite

peaks located around 787.6 and 804.1 eV further confirmed the formation of Co_3O_4 crystal phase (Li et al., 2014). The broad O 1s spectrum could be deconvoluted into three peaks, indicating three different oxygen species existed. The peak at 529.5 eV arise from lattice oxygen of the Co_3O_4 and the peaks at 531.5 and 532.3 eV can be attributed to the residual oxygen (i.e., C−O and C=O) groups on graphene surface (Fig. 2d) (Bagri et al., 2010).

3.2. Electrochemical performance of Co_3O_4@G microspheres

The electrochemical properties of the Co_3O_4@G electrode were characterized using CV under a three-electrode system using an electrolyte of alkaline solutions (0.1 M NaOH). Fig. 3a shows the CV curves of the Co_3O_4@G, Co_3O_4, and bare glassy carbon electrode (GCE) in a 0.1 M NaOH solution. Compared to bare GCE electrode, the Co_3O_4@G exhibits two pair of well-defined redox peaks, corresponding to the redox coupling of CoOOH and CoO_2. These two reversible reactions can be schematically expressed as Eqs. (1) and (2): (Ding et al., 2010)

$$Co_3O_4 + OH^- + H_2O \leftrightarrow 3CoOOH + e^- \quad (1)$$

$$CoOOH + OH^- \leftrightarrow CoO_2 + H_2O + e^- \quad (2)$$

In addition, the Co_3O_4@G electrode exhibited higher peak current and stability (< 8.7% variation after 100 cycles of CV) than Co_3O_4-modified electrodes. This indicates that hierarchical porous structures with graphene provide efficient electron and ion transport. Fig. 3b shows the CV curves of the Co_3O_4@G electrode at different scan rates. Both the oxidative and reductive peak currents (I_{pa} and I_{pc}, respectively) increased linearly with the square root of scan rate ($v^{1/2}$) with a square of regression coefficient (R^2) of 0.99 (Inset of Fig. 3b). These findings indicate a diffusion-controlled electrode process, which is an ideal case in quantitative analysis (Bard and Faulkner., 2001).

3.3. Electrocatalytic oxidation of glucose at Co_3O_4@G microspheres

The electrocatalytic activity of Co_3O_4@G towards glucose was studied by CV in 0.1 M NaOH (Fig. S6). When 4 mM glucose was added into NaOH solution, a significant oxidation peak at +0.55 V was observed because of irreversible glucose oxidation. This result is indicative of the fact that the as-prepared Co_3O_4@G exhibits strong electrocatalytic activity of glucose oxidation in alkaline solution. In contrast, no obvious response was found in bare GCE electrode in response to addition of 4 mM glucose under the same conditions. The possible mechanism of glucose oxidation with Co_3O_4@G can be shown by following reactions: (Ding et al., 2010)

$2CoO_2 + C_6H_{12}O_6$ (Glucose) $\rightarrow 2CoOOH + C_6H_{10}O_6$ (gluconolactone)

For further study of the glucose oxidation of the Co_3O_4@G electrode, we employed the in-situ Raman spectroscopy working with a customized spectroelectrochemical cell under controlled potential with addition of 20 mM glucose (Fig. 4a). As shown in Fig. 4b, peaks were observed at 195, 480, 520, 619, and 690 cm^{-1}. These peaks were assigned to the F_{2g}, E_g, F_{2g}, F_{2g} and A_{1g} vibrational modes of spinel-type Co_3O_4 respectively, which is expected to be thermodynamically stable in 0.1 M NaOH at 0 V (Yeo and Bell., 2011; Yang et al., 2010). As the potential increased to +0.55 V, the potential at which glucose oxidation occurs, the peaks related to Co_3O_4 attenuated due to conversion of Co_3O_4 to CoO_2. Following the addition of 20 mM glucose, two new peaks appeared at 497 and 556 cm^{-1} that corresponds to CoOOH (Yang et al., 2010), indicating successful oxidation of glucose on Co_3O_4@G electrode. For a clear understanding on glucose oxidation at Co_3O_4, we compared the Raman images at +0.55 V in absence and presence of glucose. The mapping image from 50 Raman spectra collected within a selected area of 5 × 5 μm^2 and band intensity of the CoOOH (green areas) at 495 ± 5 and the Co_3O_4 (red areas) at 691 ± 5 cm^{-1} (Fig. 4c–d). As shown in Fig. 4c, the dark areas newly appered due to phase transition from Co_3O_4 to CoO_2. However, the new green areas were simultaneously arised when 20 mM

glucose added, reflecting the formation of CoOOH. This result indicates that the electrochemically generated CoO_2 would act as an oxidant to oxidize glucose, which result in the regeneration of CoOOH. Consequently, this in-situ Raman study provided good evidence for the glucose oxidation on the surface of Co-based electrocatalysts, which is in good agreement with that previously proposed by voltammetric analysis (Lang et al., 2013; Ding et al., 2010).

3.4. Electrochemical biosensor for amperometric detection of glucose

The glucose sensing performance of Co_3O_4@G electrode was estimated by Co_3O_4@G-incorporated microfluidic device based on amperometric responses of glucose. The flow rate is optimized to be 500 μL min^{-1} based on the peak height and response time (~ 4 s). The oxidative current increases by successive injection of different concentration of glucose, each with 5 μL (Fig. 5a and Fig. S7). The calibration curve for the electrochemical responses of Co_3O_4@G electrode to glucose at +0.55 V (vs. Ag/AgCl) in the concentration range between 0 and 18 mM is shown in Fig. 5b. The linear relationship between the oxidation current and the glucose concentration was obtained for concentrations ranging from 0.02 to 8 mM with a correlation coefficient of 0.9994 and much higher sensitivity (628 μA mM^{-1} cm^{-2}) than the Co_3O_4 electrode(264 μA mM^{-1} cm^{-2}, R^2=0.9964). The detection limit of the Co_3O_4@G electrode was 38 nM (S/N = 3), lower than the value of Co_3O_4 electrode (97 nM). Moreover, the Co_3O_4@G electrode exhibited superior electrochemical performance of high sensitivity, wide detection range, low detection limit, and rapid response time compared to the previously other non-enzymatic metal oxide (or hydroxide) materials (Table 1). In addition, the selectivity is one of important parameters to evaluate the performance of biosensors, because the interfering species in human blood serum, such as ascorbic acid (AA), uric acid (UA), and dopamine (DA) might interfere with the glucose sensing. The selectivity of Co_3O_4@G for detecting glucose was

investigated by consecutive injection of 3 mM glucose, 0.2 mM AA, 0.2 mM UA, and 0.2 mM DA at an applied potential of +0.55 V (Fig. 5c). The strong current responses for glucose were observed while the small current responses were observed for AA, UA, and DA. Compared to 3 mM glucose, these current responses can be neglected. This indicates that the Co_3O_4@G has good selectivity against some of the main interfering molecules.

3.5. Stability, reproducibility, and the practical test

The long-term staibility of the Co_3O_4@G electrode toward glucose oxidation was also tested (Fig. S8). When the Co_3O_4@G electrode was not used, it was stored in air at room temperature. The amperometric response of the electrode were found to be stable, keeping 97.3% of its initial intensity. Replicate injection of glucose have been evaluated acceptable repeatability; the current signals still maintained after 50 cycles of glucose detection (Fig. 5d). For prctical test, human blood serum samples were measured by Co_3O_4@G-based biosensors. The concentration of glucose in the serum sample was calibrated using standard glucose solution and compared with the result obtained by the ACCU-CHEK® Performa Blood Glucose Meter. As presented in Table S1, the results from the biosensors are similar to those tested by the glucose meter, indicating the as-prepared biosensor may hold potential in real sample analysis.

3.6. Study of Electrochemical Kinetics in Co_3O_4@G Microspheres.

Study of electrochemical kinetics in Co_3O_4@G microspheres An understanding of enhanced electrochemical kinetics in Co_3O_4@G is essential in a view of fundamental science and practical applications. Chronoamperometry and EIS were employed in order to gain insight into electrochemical behavior of the Co_3O_4@G electrode. The catalytic rate constant (k_{cat}) for the oxidation of glucose was determined with chronoamperometry. Fig. 6a shows chronoamperograms of Co_3O_4@G electrode in 0.1 M NaOH solution in absence and presence of

glucose. At intermediate time used in this study, the catalytic current is dominated by the rate of the electrocatalytic oxidation of glucose, and the rate constant for chemical reaction between glucose and Co_3O_4@G was determined as follows: (Yu et al., 2013)

$$\frac{I_{cat}}{I_L} = \pi^{1/2}(k_{cat}Ct)^{1/2}$$

where I_{cat} and I_L is the currents in presence and absence of glucose, respectively; k_{cat}, C, and t are the catalytic rate constant (M^{-1} s^{-1}), the bulk concentration (M) of glucose and time elapse (s). From the slope of I_{cat}/I_L versus $t^{1/2}$, the k_{cat} of Co_3O_4@G electrode was estimated to be 3.45×10^4 M^{-1} s^{-1}, while that of Co_3O_4 electrode was 2.18×10^4 M^{-1} s^{-1} (Fig. S9). The k_{cat} value of our Co_3O_4@G microsphere is comparable or even higher than those of previously reported CoO_x nanocluster/overoxidized polypyrrole composite (5.1×10^4 M^{-1} s^{-1}) (Yu et al., 2013), Cu_2O/Cu (4.02×10^4 M^{-1} s^{-1}) (Wang et al., 2012), CoO/G microsphere (1.42×10^4 M^{-1} s^{-1}) (Ci et al., 2014), 3D porous Ni nanostructures (1.20×10^3 M^{-1} s^{-1}) (Niu et al., 2013).

EIS was further performed to evaluate the charge transfer resistance of electrode materials at +0.55 V in 4 mM glucose. Fig. 6b shows the Nyquist plots obtained for each modified electrode surface. The semicircle at the high frequency region is due to charge transfer and the one at the low frequency region is due to the adsorption of the intermediates. In the equivalent circuit, R_s represents the solution resistance, R_{ct} represents the charge-transfer resistance, CPE is the constant-phase element, and Z_W is the Warburg element (Choi et al., 2010). The Co_3O_4@G electrode represent lower R_{ct} value for glucose oxidation than that of Co_3O_4 electrode. This result indicates that hierarchical networks and Co_3O_4-graphene sandwich-like structure provide efficient diffusion of analytes by shortening diffusion path facilitate electron transfer, leading to the enhanced electrocatalytic glucose oxidation.

4. Conclusions

We developed the preparation of hierarchical porous Co_3O_4@G microspheres comprised of Co_3O_4 and graphene sheets by one-step hydrothermal treatment. As-prepared hierarchical microspheres exhibited a uniform flower-like structure with an average diameter of 8.2 ± 1.6 μm. Using the Co_3O_4@G microspheres, we fabricated flow-injection microfluidic system for detection of glucose, showing outstanding performance of high sensitivity, low detection limit, and rapid response time. The hierarchical porous architecture provided large accessible area of Co_3O_4 active sites with facilitated ion transfer, while the interconnected graphene nanosheets offered continuous electron pathways for efficient electroactive Co_3O_4. We anticipate that such design and fabrication of hierarchical porous Co_3O_4@G microspheres will be applicable to more extensive nanocomposites that could resolve limited ion and electron transfer in electrochemical applications such as lithium ion batteries, supercapacitors, and electrochemical biosensors.

Acknowledgements

This work was supported by the National Research Foundation of Korea (NRF) Grant funded by the Korean Government (MSIP) (No. 2014R1A5A2010008) and the BioNano Health-Guard Research Center funded by the Ministry of Science, ICT & Future Planning (MSIP) of Korea, Global Frontier Project (Grant number H-GUARD_2013M3A6B2078945).

References

Baghayeri, M., Veisi, H., 2015. Biosens. Bioelectron. 74 (15), 190–198.

Bagri, A., Mattevi, C., Acik, M., Chabal, Y. J., Chhowalla, M., Shenoy, V. B., 2010. Nat. Chem. 2 (7), 581–587.

Bard, J., Faulkner, L. R., 2001. Wiley, New York.

Cao, H., Xiao, F., Ching, C. B., Duan, H., 2011. ACS Appl. Mater. Interfaces 3 (8), 3049–3057.

Cao, X., Wang, N., Jia, S., Shao, Y., 2013. Anal. Chem. 85 (10), 5040–5046.

Chen, C., Xie, Q., Yang, D., Xiao, H., Fu, Y., Tan, Y., Yao, S., 2013. RSC Adv. 3 (14), 4473–4491.

Cheng, T.-M., Huang, T.-K., Lin, H.-K., Tung, S.-P., Chen, Y.-L., Lee, C.-Y., Chiu, H.-T., 2010. ACS Appl. Mater. Interfaces 2 (10), 2773–2780.

Chen, X.-M., Lin, Z.-J., Chen, D.-J., Jia, T.-T., Cai, Z.-M., Wang, X.-R., Chen, X., Chen, G.-N., Oyama, M., 2010. Biosens. Bioelectron. 25 (7), 1803–1808.

Choi, B. G., Park, H., Park, T. J., Yang, M. H., Kim, J. S., Jang, S.-Y., Heo, N. S., Lee, S. Y., Kong, J., Hong, W. H., 2010. ACS Nano 4 (5), 2910–2918.

Ci, S., Mao, S., Huang, T., Wen, Z., Steeber, D. A., Chen, J., 2014. Electroanalysis 26 (6), 1326–1334.

Cong, H.-P., Chen, J.-F., Yu, S.-H., 2014. Chem. Soc. Rev. 43 (21), 7295–7456.

Dai, G., Lu, P., Iiang, Y., Lei, Y., 2013. J. Chin. Chem. Soc. 60 (4), 366–370.

Ding, Y., Wang, Y., Su, L., Bellagamba, M., Zhang, H., Lei, Y., 2010. Biosens. Bioelectron. 26 (2), 542–548.

Dong, X.-C., Xu, H., Wang, X.-W., Huang, Y.-X., Chan-Park, M.B., Zhang, H., Wang, L.-H., Huang, W., Chen, P., 2012. ACS Nano 6 (4), 3206–3213.

Gao, Z.-D., Guo, J., Shrestha, N. K., Hahn, R., Song, Y.-Y., Schmuki, P., 2013. Chem. Eur. J. 19 (46), 15530–15534.

Gao, Z. D., Han, Y., Wang, Y., Xu, J., Song, Y.-Y., 2013. Sci. Rep. 3, 3323–3329.

Hamon, C., Novikov, S., Scarabeli, L., Basabe-Desmonts, L., Liz-Marzán, L. M., 2014. ACS Nano 8 (10), 10694–10703.

Hoa, L.T., Chung, J.S., Hur, S.H., 2016. Sens. Actuators B: Chem. 233, 76–82.

Hou, C., Xu, Q., Yin, L., Hu, X., 2012. Analyst 137 (24), 5803–5808.

Hu, Z., Chen, G., 2014. Adv. Mater. 26 (34), 5950–5956.

Ibupoto, Z. H., Khun, K., Beni, V., Liu, X., Willander, M., 2013. Sensors 13 (6), 7926–7938.

Kung, C.-W., Lin, C.-Y., Lai, Y.-H., Vittal, R., Ho, J.-C., 2011. Biosens. Bioelectron. 27 (1), 125–131.

Lang, X.-Y., Fu, H.-Y., Hou, C., Han, G.-F., Yang, P., Liu, Y.-B., Jiang, Q., 2013. Nat. Commun. 4, 2169–2177.

Lee, K. K., Loh, P. Y., Sow, C. H., Chin, W. S., 2012. Electrochem. Commun. 20 (1), 128–132.

Li, L., Liu, M., He, S., Chen, W., 2014. Anal. Chem. 86 (15), 7996–8002.

Li, M., Han, C., Zhang, Y., Bo., X., Guo, L., 2015. Anal. Chim. Acta 861, 25–35.

Mu, Y., Jia, D., He, Y., Miao, Y., Wu, H.-L., 2011. Biosens. Bioelectron. 26 (6), 2948–2952.

Niu, X., Lan, M., Zhao, H., Chen, C., 2013. Anal. Chem. 85 (7), 3561–3569.

Park, S., Chung, T. D., Kim, H. C., 2003. Anal. Chem. 75 (13), 3046–3049.

Reitz, E., Jia, W., Gentile, M., Wang, Y., Lei, Y., 2008. Electroanlaysis 20 (22), 2482–2486.

Si, P., Dong, X.-C., Chen, P., Kim, D.-H., 2013. J. Mater. Chem. B 1 (48), 110–115.

Si, P., Huang, Y., Wang, T., Ma, J., 2013. RSC Adv. 3 (12), 3487–3847.

Sumathi, C., Muthukumaran, P., Radhakrishnan, S., Wilson, J., Umar, A., 2014. RSC Adv. 4 (44), 23050–23057.

Toghill, K. E., Compton, R. G., 2010. J. Electrochem. Sci. 5, 1246–1301.

Wang, J., Thomas, D. F., Chen, A., 2008. Anal. Chem. 80 (4), 997–1004.

Wang, L., Fu, J., Hou, H., Song, Y., 2012. Int. J. Electrochem. Sci. 7, 12587–12600.

Wang, L., Ye, Y., Shen, Y., Wang, F., Lu, X., Xie, Y., Chen, S., Tan, H., Xu, F., Song, Y., 2014. Sens. Actuators B: Chem. 203, 864–872.

Wang, X., Dong, X., Wen, Y., Li, C., Xiong, Q., Chen, P., 2012. Chem. Commun. 48, 6490–6492.

Wilson, R., Turner, A. P. F., 1992. Biosens. Bioelectron. 7 (3), 165–185.

Xiao, F., Li, Y., Zan, X., Liao, K., Xu, R., Duan, H., 2012. Adv. Funct. Mater. 22 (12), 2487–2494.

Xiao, F., Zhao, F., Mei, D., Mo, Z., Zeng, B., 2009. Biosens. Bioelectron. 24 (12), 3481–3486.

Yang, D., Velamakanni, A., Bozoklu, G., Park, S., Stoller, M., Piner, R. D., Stankovich, S., Jung, I., Field, D. A., Ventrice Jr. C. A., Ruoff, R. S., 2009. Carbon 47 (1), 145–152.

Yang, J., Liu, H., Martens, W. N., Frost, R. L., 2010. J. Phys. Chem. C 114 (1), 111–119.

Yeo, S., Bell, A. T., 2011. J. Am. Chem. Soc. 133 (14), 5587–5593.

Yue, H. Y., Huang, S., Chang, J., Heo, C., Yao, F., Adhikari, S., Gunes, F., Liu, L. C., Lee, T. H., Oh, E. S., Li, B., Zhang, J. J., Huy, T. Q., Luan, N. V., Lee, Y. H., 2014. ACS Nano 8 (2), 1639–1646.

Yu, H., Jin, J., Jian, X., Wang, Y., Qi, G.-C., 2013. Electroanlaysis 25 (7), 1665–1674.

Zeng, Q., Cheng, J., Tang, L., Liu, X., Liu, Y., Li, J., Jiang, J., 2010. Adv. Funct. Mater. 20 (19), 3366–3372.

Zheng, Y., Li, P., Li, H., Chen, S., 2014. Int. J. Electrochem. Sci. 9, 7369–7381.

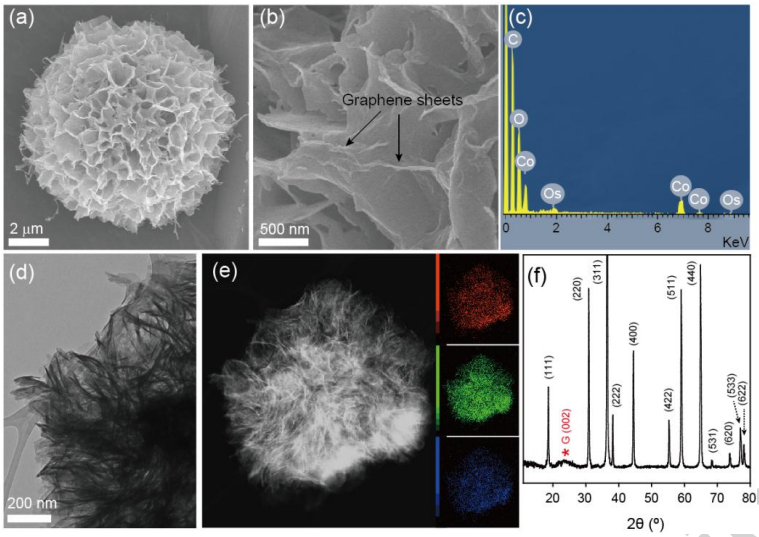

Fig. 1. (a) Low magnification and (b) high-magnification SEM images of hierarchical Co_3O_4@G microsphere. (c) The EDS analysis on selected areas. (d) TEM image of hierarchical Co_3O_4@G microsphere. (e) The EDS mapping of C (red), O (green), and Co (blue) elements of hierarchical Co_3O_4@G microsphere. (f) XRD pattern of hierarchical Co_3O_4@G microspheres.

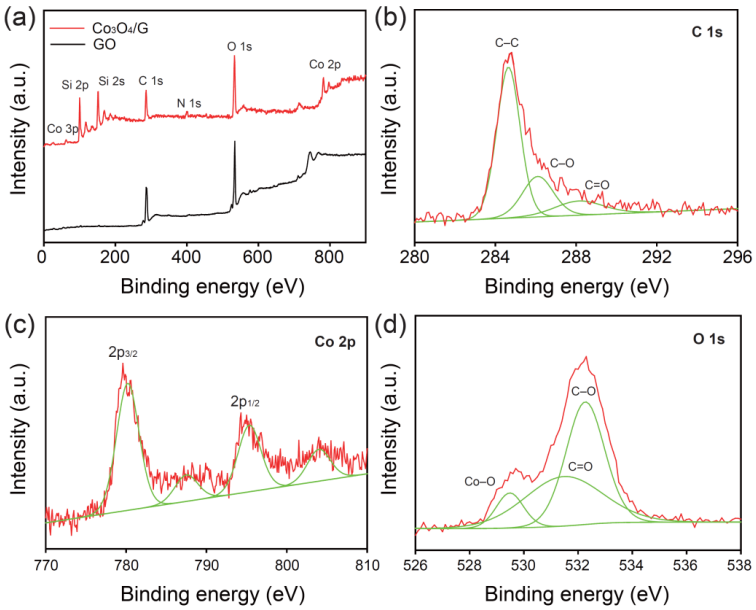

Fig. 2. (a) XPS survey spectra obtained from hierarchical Co_3O_4@G microspheres and GOs. (b) C 1s, (d) Co 2p, and (d) O 1s core level XPS spectra of hierarchical Co_3O_4@G microspheres.

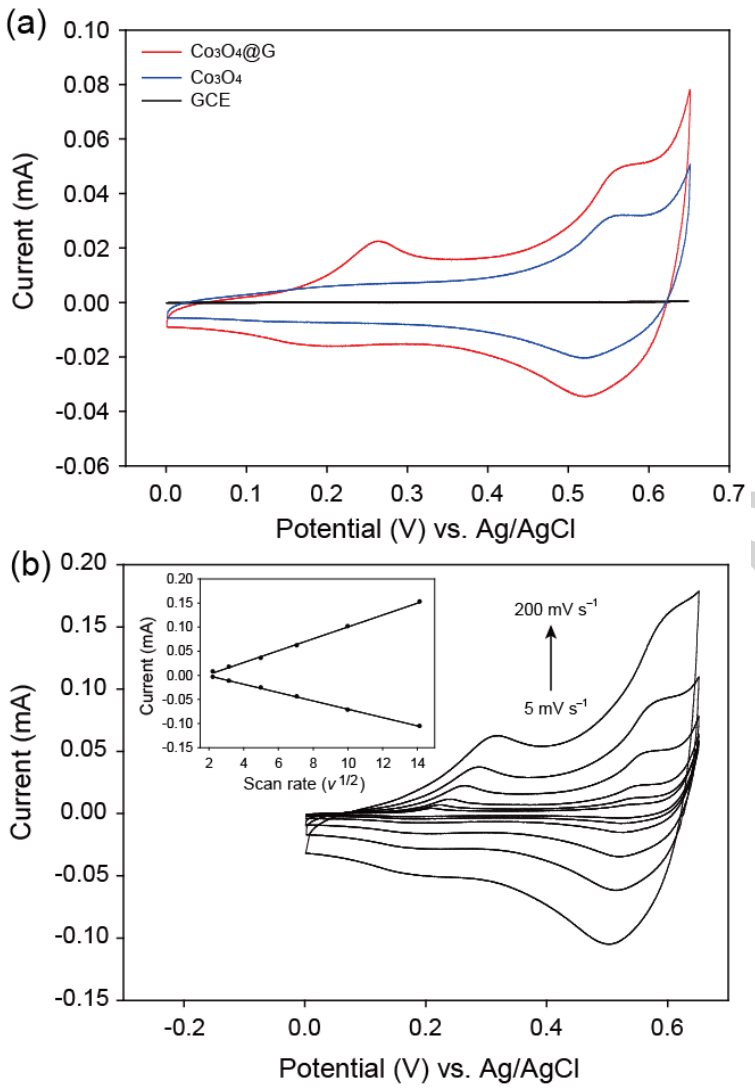

Fig. 3. (a) Cyclic voltammograms of bare GCE (black line), Co_3O_4 nanoparticles (blue line), and hierarchical Co_3O_4@G microspheres (red line)-modified electrode. (b) Cyclic voltammograms of hierarchical Co_3O_4@G microspheres at various scan rates from 5, 10, 20, 50, 100, and 200 mV s^{-1}, respectively. Inset: plot of peak current vs. square root of scan rate.

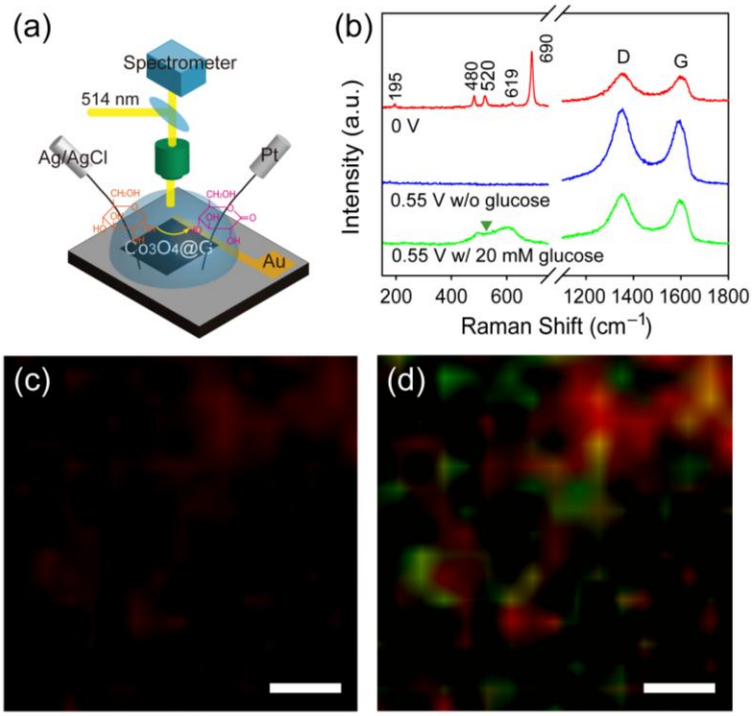

Fig. 4. (a) Schematic images of in-situ Raman spectroscopy. (b) In-situ Raman spectra of hierarchical Co_3O_4@G microsphere in absence and in presence of 20 mM glucose under controlled potential. (c and d) Overlay of the Raman maps of CoOOH (495 cm^{-1}) and Co_3O_4 (691 cm^{-1}) at +0.55 V in presence and absence of 20 mM glucose, respectively.

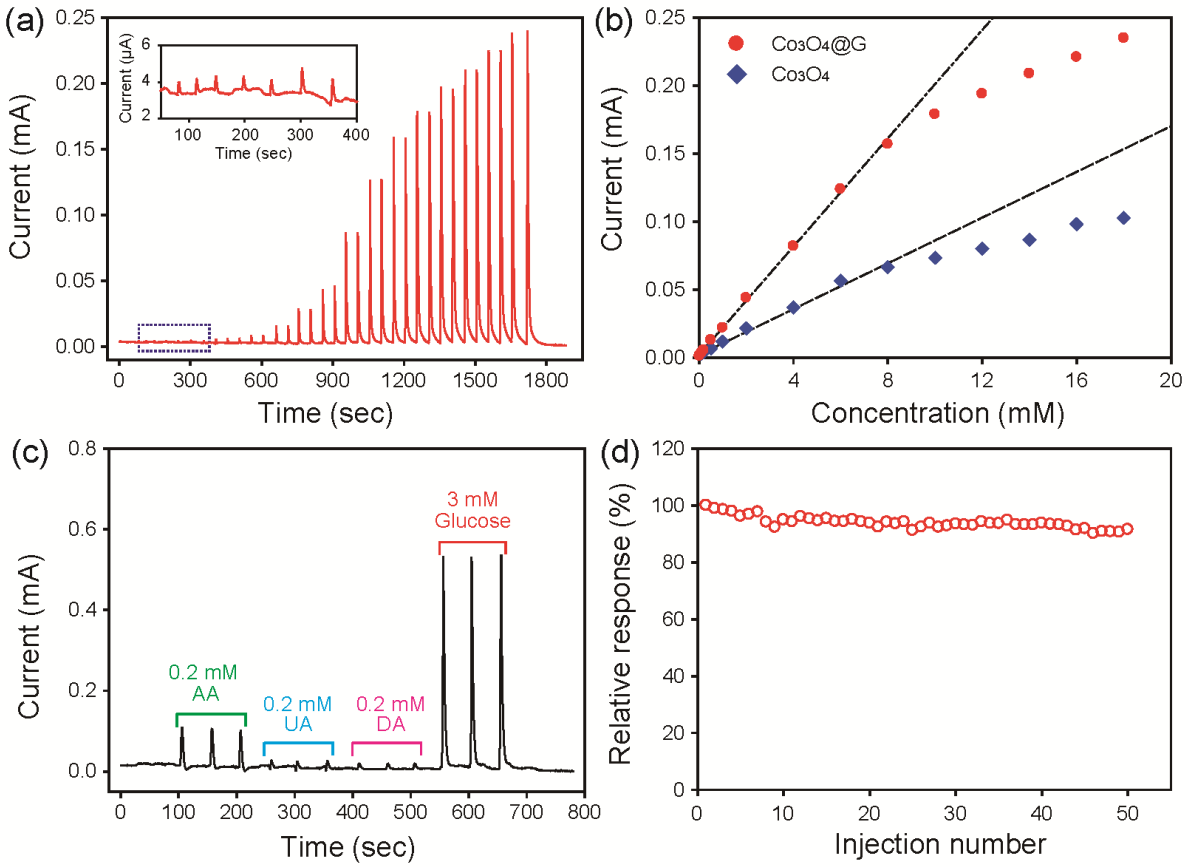

Fig. 5. (a) Amperometric responses of hierarchical Co_3O_4@G modified electrode (holding at +0.55 V) to subsequent injection of glucose with increasing concentrations of 0.02 to 18 mM. Inset: amplified response curves for injection of 0.02 and 0.1 mM glucose. (b) The calibration curves for the amperometric responses of hierarchical Co_3O_4@G and Co_3O_4 modified electrode. (c) Amperometric responses to the successive addition of interfering compounds, such as 0.2 mM ascorbic acid, 0.2 mM uric acid, 0.2 mM dopamine as well as 3 mM glucose. (d) Variation of the response current of the enzyme-free glucose sensor to 5 mM glucose with injection number.

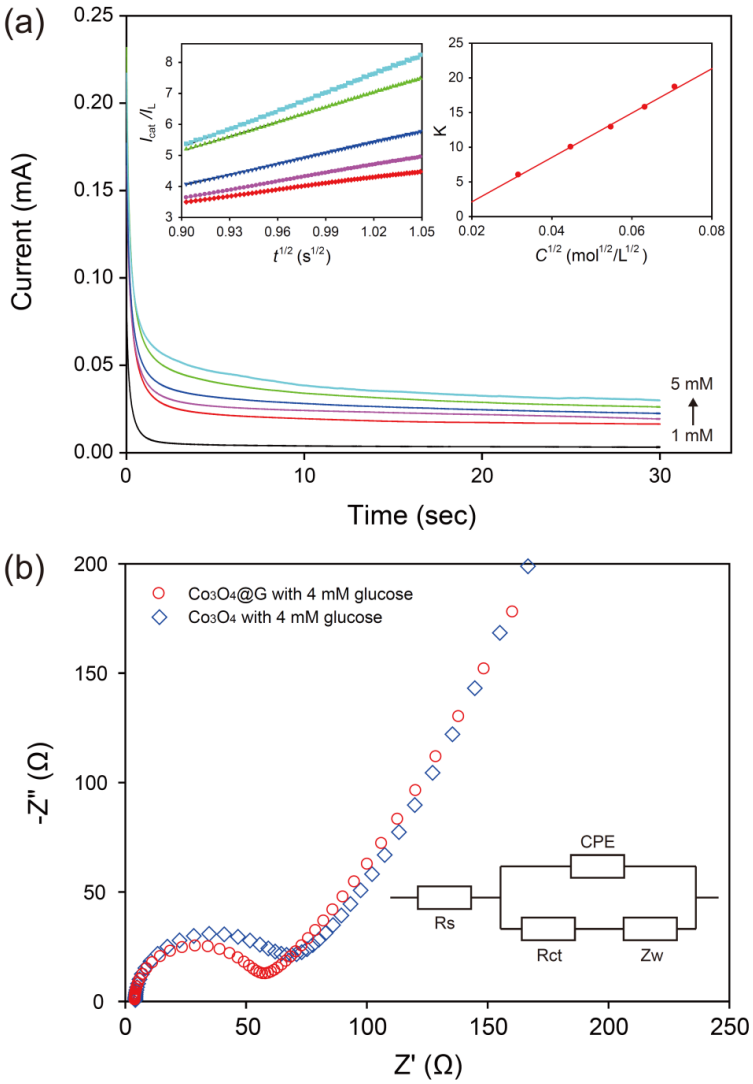

Fig. 6. (a) Chronoamperomeric plots of the hierarchical Co_3O_4@G microsphere modified electrode with different concentration of glucose in 0.1 M NaOH recorded at +0.55 V. Insets are plots of I_{cat}/I_L versus $t^{1/2}$ (left) and plots of slopes (K) from the left graph versus $C^{1/2}$. (b) Nyquist plots of hierarchical Co_3O_4@G microsphere and Co_3O_4 modified electrode with 4 mM glucose in 0.1 M NaOH recorded at +0.55 V.

Table 1. Comparison of sensing performance of the different enzyme-free glucose biosensors.

Electrode	Sensitivity ($\mu A\ mM^{-1}\ cm^{-2}$)	Linear range (mM)	Detection limit (μM) (S/N = 3)	Response time (s)	Reference
CuO nanosheets	520	0.5–10	0.1	NR	(Ibupoto et al., 2013)
CuO nanospheres	404.53	0.05–2.55	1.0	NR	(Reitz et al., 2008)
CoO nanorods	571.8	0.2–3.5	0.058	20–40	(Kung et al., 2011)
Co_3O_4 nanofibers	36.25	0.004–8	0.97	<7	(Ding et al., 2010)
Co_3O_4 nanoparticles	520.7	0.005–0.8	0.13	<6	(Hou et al., 2012)
Co_3O_4 nanoflower/GOH[a]	429.8	0.25–10	NR	8	(Hoa et al., 2016)
Co_3O_4/Graphene	20.1	0.09–6.03	0.52	NR	(Dai et al., 2013)
Co_3O_4-RGO[b]	506.5	1.0–6.5	0.01	3	(Li et al., 2015)
Co_3O_4/Graphene	NR	0.05−0.3	10	NR	(Wang et al., 2012)
CoOOH nanosheets	314	0.03–0.7	30.9	<4	(Lee et al., 2012)
$Ni(OH)_2/TiO_xC_y$	240	0.02–11.0	5.0	5	(Gao et al., 2013)
NiO/TiO_2	252.0	0.005–12.1	1.0	NR	(Gao et al., 2013)
Co_3O_4@G microspheres	628	0.02–8	0.038	4	This work

[a]Graphene oxide hydrogel.
[b]Reduced graphene oxide.

Electronic Support Information (ESI)

Hierarchical porous microspheres of the Co_3O_4@graphene with enhanced electrocatalytic performance for electrochemical biosensors

MinHo Yang, Jae-Min Jeong, Kyoung G. Lee, Do Hyun Kim, Seok Jae Lee,* and Bong Gill Choi*

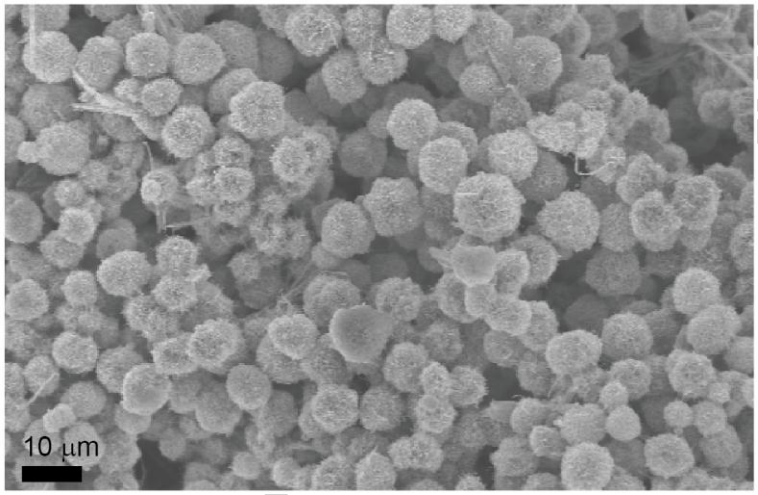

Fig. S1. SEM image of hierarchical porous Co_3O_4@G microspheres.

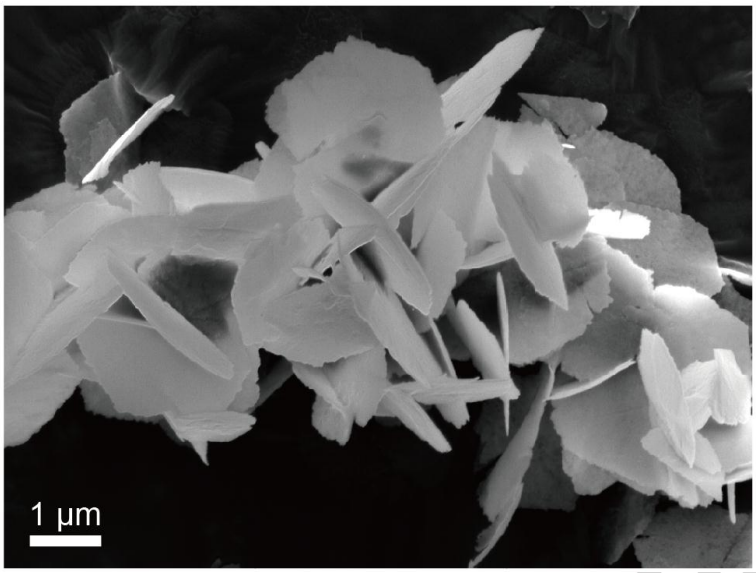

Fig. S2. SEM image of Co_3O_4 sheets.

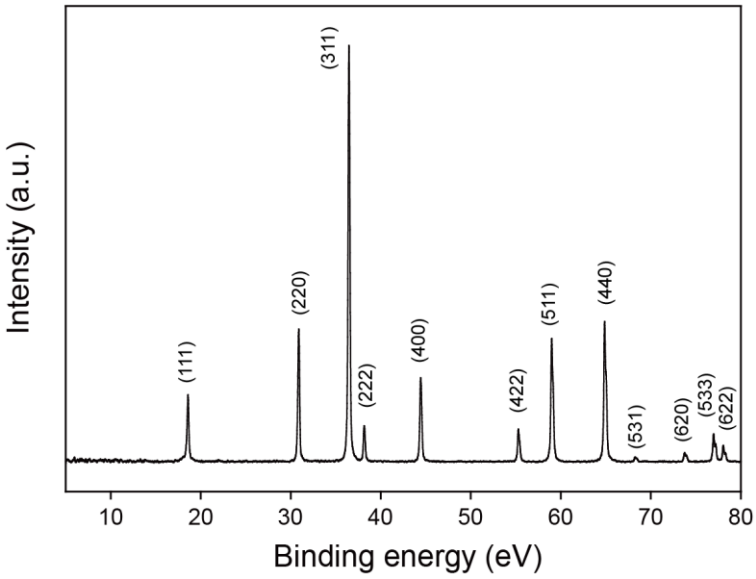

Fig. S3. XRD pattern of Co_3O_4 sheets.

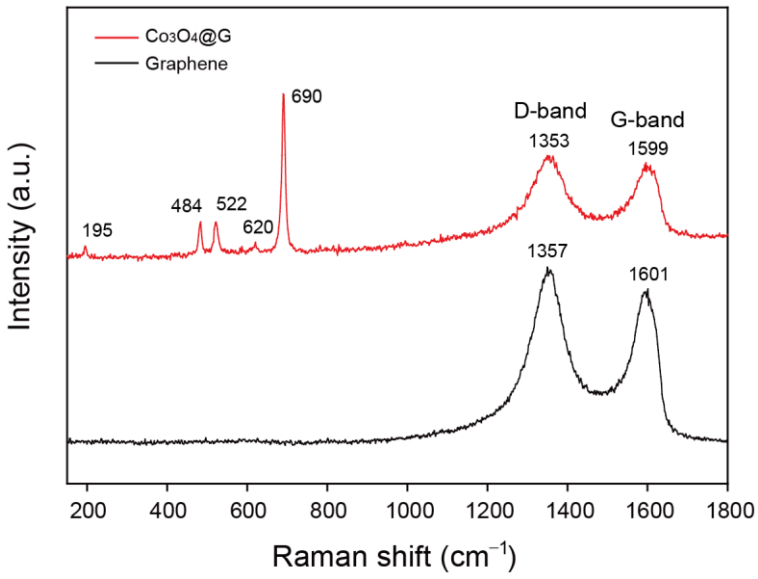

Fig. S4. Raman spectra of Co_3O_4@G and graphene samples.

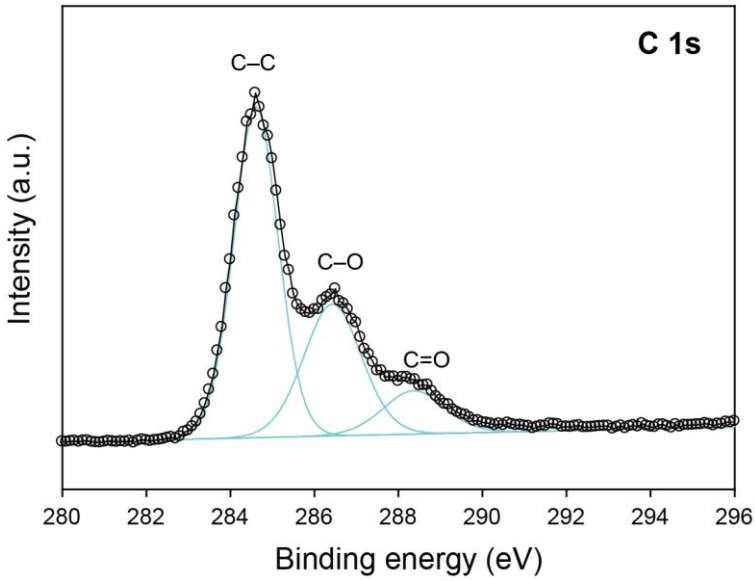

Fig. S5. C 1s core level XPS spectra of GOs.

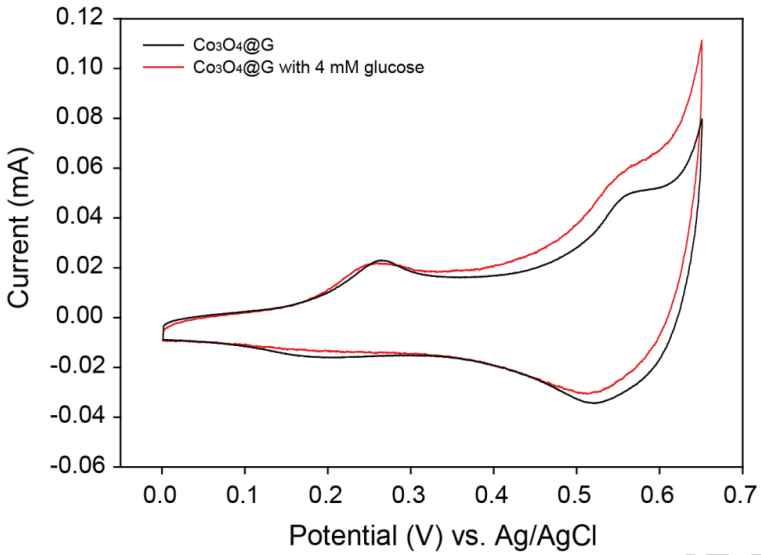

Fig. S6. Cyclic voltammograms at hierarchical Co_3O_4@G microspheres modified electrodes in 0.1 M NaOH solution in the absence (black line) and in the presence (red line) of 4 mM glucose. Scan rate of 50 mV s^{-1}.

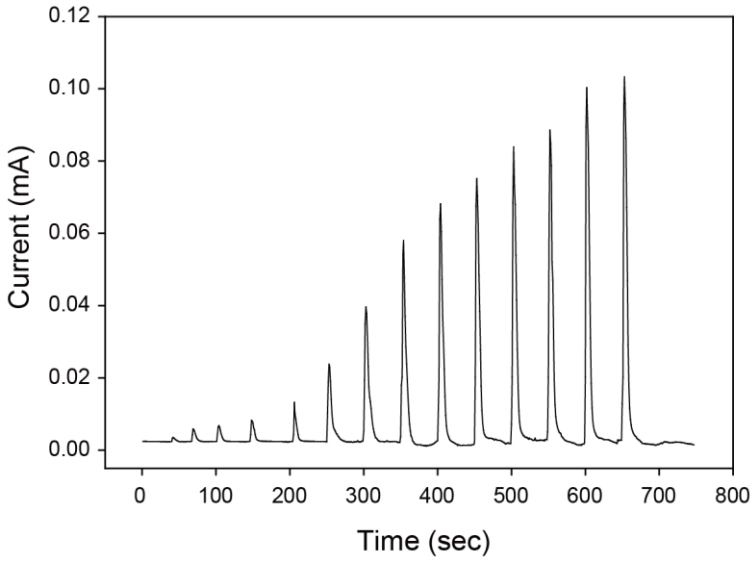

Fig. S7. Amperometric responses of Co_3O_4 modified electrode (holding at +0.55 V) to subsequent injection of glucose with increasing concentrations of 0.02 to 18 mM.

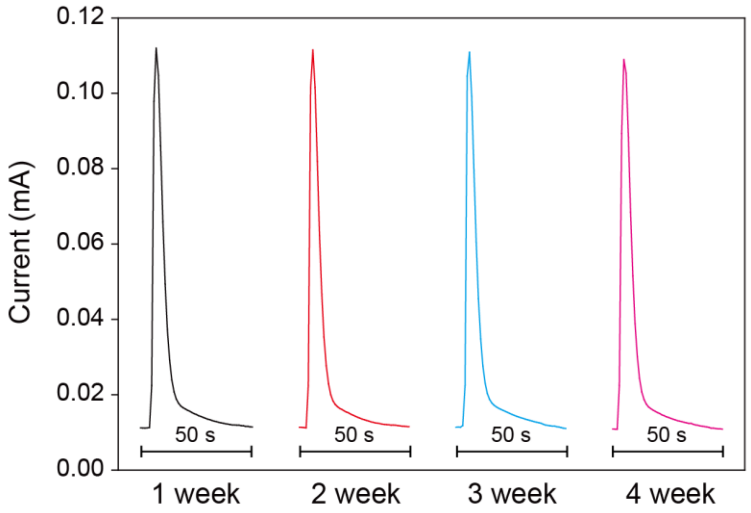

Fig. S8. Amperometric responses of Co_3O_4@G electrode to 5 mM of glucose at +0.55 V. The current responses were measured every week until the fourth week.

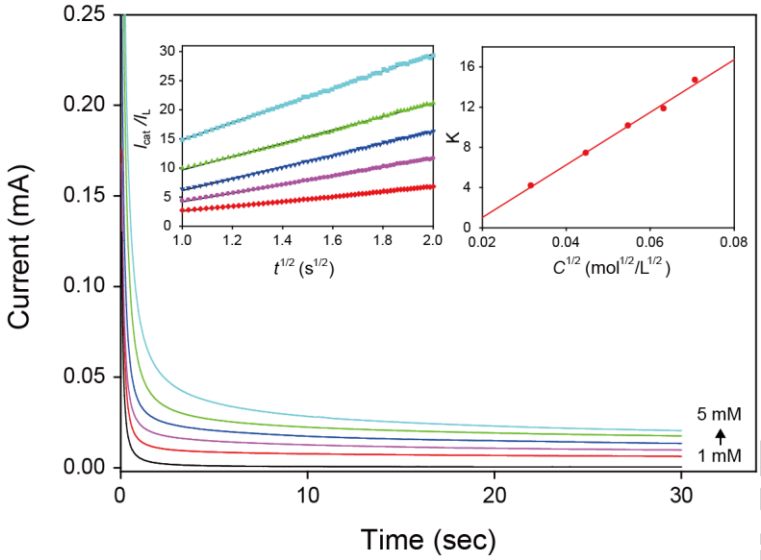

Fig. S9. Chronoamperomeric plots of the Co_3O_4 modified electrode with different concentration of glucose in 0.1 M NaOH recorded at +0.55 V. Insets are plots of I_{cat}/I_L versus $t^{1/2}$ (left) and plots of slopes (K) from the left graph versus $C^{1/2}$.

Table S1. Determination of glucose in human blood serum samples.

Sample	Glucose meter	Co_3O_4@G	RSD (%) (n=3)
1	6.28 mM	6.24 mM	2.26
2	5.61 mM	6.69 mM	2.12
3	6.00 mM	6.10 mM	3.63

Highlights

• Preparation of hierarchical, porous, and hybrid structured microspheres using a one-step hydrothermal method.

• Analysis of electrochemical behavior (i.e. reaction kinetics, interfacial charge transfer, and sensing mechanism) of Co_3O_4@Graphene microsphere electrodes.

• Fabrication of microfluidic enzyme-free biosensor for detection of glucose, showing high sensitivity (628 μA mM^{-1} cm^{-2}), low detection limit (38 nM), fast response (within 4 s), and high selectivity.

Graphical abstract

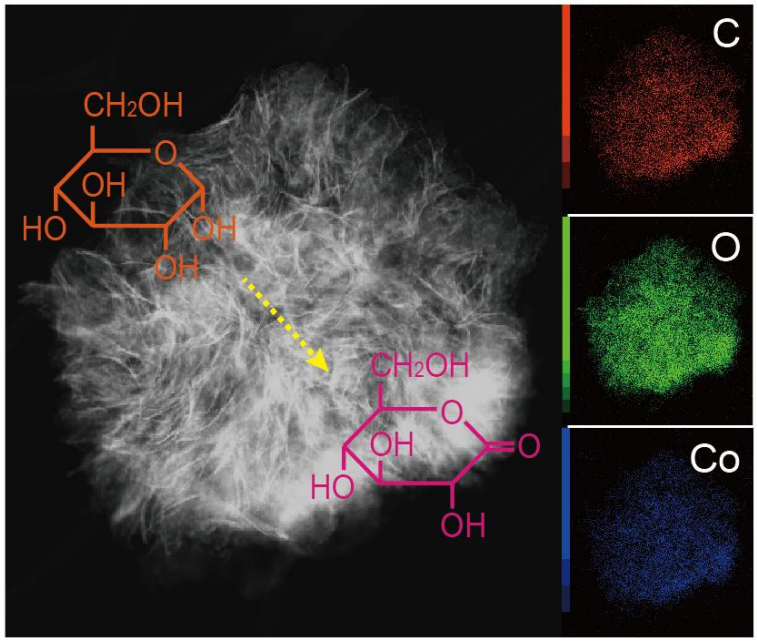

Highlights

• Preparation of hierarchical, porous, and hybrid structured microspheres using a one-step hydrothermal method.

• Analysis of electrochemical behavior of Co_3O_4@Graphene microsphere electrodes.

• Fabrication of microfluidic enzyme-free biosensor for detection of glucose, showing high sensitivity, low detection limit, fast response, and high selectivity.

Graphical abstract